Model-Based Reconstructive Elasticity Imaging of Deep Venous Thrombosis

Salavat Aglyamov, Andrei R. Skovoroda, Jonathan M. Rubin, *Member, IEEE*, Matthew O'Donnell, *Fellow, IEEE*, and Stanislav Y. Emelianov, *Member, IEEE*

***Abstract*—Deep venous thrombosis (DVT) and its sequela, pulmonary embolism, is a significant clinical problem. Once detected, DVT treatment is based on the age of the clot. There are no good noninvasive methods, however, to determine clot age. Previously, we demonstrated that imaging internal mechanical strains can identify and possibly age thrombus in a deep vein. In this study the deformation geometry for DVT elasticity imaging and its effect on Young's modulus estimates is addressed. A model-based reconstruction method is presented to estimate elasticity in which the clot-containing vessel is modeled as a layered cylinder. Compared to an unconstrained approach in reconstructive elasticity imaging, the proposed model-based approach has several advantages: only one component of the strain tensor is used; the minimization procedure is very fast; the method is highly efficient because an analytic solution of the forward elastic problem is used; and the method is not very sensitive to the details of the external load pattern—a characteristic that is important for free-hand, external, surface-applied deformation. The approach was tested theoretically using a numerical model, and experimentally on both tissue-like phantoms and an animal model of DVT. Results suggest that elasticity reconstruction may prove to be a practical adjunct to triplex scanning to detect, diagnose, and stage DVT.**

I. Introduction

In previous publications [1]–[3] we have demonstrated that imaging internal mechanical strains not only identifies thrombus in a deep vein, but also it may be able to age the thrombus. In particular, we have proposed a triplex ultrasound imaging method combining conventional B-scan and blood flow modalities with elasticity scanning to detect, diagnose, and stage deep venous thrombosis (DVT) [3].

Deep venous thrombosis, and its sequela, pulmonary embolism, is a significant clinical problem, representing the leading cause of preventable, in-hospital mortality in the United States and other developed countries [4]. The symptomatic indication of DVT is always confirmed by objective tests; the most common test is duplex ultrasound combining gray-scale, color-flow Doppler, and compression ultrasound [5]. In previous studies [3], we demonstrated that high-quality strain images can be obtained during venous compressional ultrasound. Moreover, if the deformation geometry is carefully controlled, these images alone can differentiate acute from chronic DVT.

The distinction between acute and chronic DVT is clinically important. A patient with acute DVT is treated with heparin followed by oral anticoagulants, and one with chronic DVT is treated with oral anticoagulants alone because the stronger anticoagulant and anti-inflammatory effects of heparin are not required [6]. Furthermore, one would like to avoid the use of heparin if at all possible. Heparin is a powerful anticoagulant that must be injected, and it has a higher risk of bleeding than oral anticoagulants. In fact, studies have shown that the risk of bleeding with heparin is 11% during the first 5 to 10 days of therapy [7]. Consequently, translating our initial findings into a robust, reproducible elasticity imaging technique to age DVT will have an immediate and significant clinical impact.

In this study, we address DVT reconstructive elasticity imaging and how the geometry of the clot containing vein and surrounding tissue affects elasticity estimates. To make triplex ultrasound a routine clinical procedure, elasticity information most probably will be acquired during free-hand scanning and compression. To test for a blood clot in the femoral vein, for example, compression ultrasound is performed by "marching down" a subject's leg, imaging the femoral vein in transverse orientation while simultaneously deforming the vein with the scanhead [2], [3]. If a venous thrombus is not present, the walls of the vein quickly coapt before the adjacent artery collapses. If a thrombus is present, the arterial walls coapt before the vein's [5]. A clot can extend for a few up to many centimeters along the vein. Using visual feedback from real-time ultrasound images, the applied deformation can be controlled to approximate a plane strain state through the cross section of a vein with an elongated clot. However, the in-plane deformation geometry is very hard to control using free-hand scanning.

The effects of geometry and boundary conditions on DVT elasticity images was analyzed using a simple model of thrombus elasticity. The vein containing the clot is modeled as an inhomogeneous elastic cylinder inside incom-

Manuscript received October 1, 2002; accepted October 30, 2003. Financial support from the National Institutes of Health under grants HL47401, DK47324, HL67647, CA69568, and HL68658.

S. Aglyamov, M. O'Donnell, and S. Y. Emelianov are with the Department of Biomedical Engineering, University of Michigan, Ann Arbor, MI 48109 (e-mail: emelian@mail.utexas.edu).

J. M. Rubin is with the Department of Radiology, University of Michigan, Ann Arbor, MI 48109.

S. Aglyamov is also with the Institute of Mathematical Problems of Biology, Russian Academy of Sciences, Pushchino, Moscow Region, Russia 142290.

A. R. Skovoroda was with the Department of Biomedical Engineering, University of Michigan, Ann Arbor, MI 48109 and the Institute of Mathematical Problems of Biology, Russian Academy of Sciences, Pushchino, Moscow Region, Russia 142290.

pressible surrounding tissue, where the Young's modulus of the object (clot, vein, and surrounding tissue) is assumed to be an unknown function of spatial coordinates. More precisely, the vein containing the clot is approximated by an inhomogeneous cylinder with modulus being only a function of the radial coordinate. After developing this model in Section II, we demonstrate that uncontrolled in-plane deformations can lead to greatly reduced contrast in normal strain images. This result strongly implies that strain images alone cannot differentiate acute from chronic DVT if the in-plane deformation is not carefully controlled.

Using this same model, we also derive the solution to the forward elastic problem for an arbitrary planar deformation (i.e., superposition of uniaxial and shear loads). This general analytic solution then is used to reconstruct the unknown Young's modulus of the object in a region of interest (ROI) based on the iterative comparison of theoretically predicted and ultrasonically measured longitudinal strain tensor components. The Young's modulus distribution providing the best agreement is assumed as the distribution of elastic properties inside the clot, vein wall, and surrounding tissue. This reconstruction procedure can overcome the limitations of strain imaging for an arbitrary in-plane deformation.

The proposed approach is tested first using numerically simulated inhomogeneous objects modeling the clot. Maps of the longitudinal component of the strain tensor are input to the elasticity reconstruction procedure. Reconstructed elasticity images are shown to closely match the initially prescribed elastic properties of the vein wall, clot, and surrounding tissue.

The reconstruction procedure then is tested using measured maps of the longitudinal component of the strain tensor acquired from tissue-equivalent phantoms approximating the three-component clot model in which the vein contains either an acute (soft) or chronic (hard) clot. The reconstructed Young's modulus distribution is compared with the results of direct measurements of the elastic properties of the phantom materials. Again, reconstructed elasticity images closely match predictions.

The reconstruction procedure is tested using longitudinal strain tensor fields measured in an animal model (Sprague-Dawley rats) of DVT. Results of reconstructed relative elasticity distributions clearly show that acute and chronic clots can be differentiated. The paper concludes with a discussion of the applicability of the proposed reconstruction methods to triplex scanning procedures to detect, diagnose, and stage DVT in the clinic.

II. Theory

A. Forward Problem

Elasticity reconstruction can be posed in many different ways. In general, all displacement and strain components are needed to reconstruct the spatial distribution of the Young's modulus [8]–[11]. Unlike many other applications, however, the geometry for DVT reconstruction is well defined. The shape, location, and margins of the vessel containing the clot are well-known from B-scan images. Therefore, a model-based approach with a reduced set of unknown parameters may prove useful for this application to reconstruct the spatial elasticity distribution over a small ROI containing the vessel with the clot.

Here we assume that the clot-containing vessel can be modeled as a long cylinder (i.e., cylinder length at least several times larger than the cross-sectional diameter of the vessel). We use a cylindrical coordinate system (r, ϕ, z), in which the origin of the coordinate system is placed at the center of a cylindrically symmetric vessel, and the z-axis is aligned parallel with the vessel's longitudinal axis. For this configuration, the elastic modulus distribution across the imaging plane is assumed simply to be a function of radial position over a small region of interest around the clot. External loading does not vary, or changes very slowly, along the length of the cylinder such that the out-of-plane displacement u_z is either zero or small compared to the other two displacement components (radial u_r and azimuthal u_φ), and the in-plane displacement components do not vary significantly as a function of the out-of-plane coordinate z. That is, we assume a plane strain state [12]. Based on previous experimental studies on both an animal model of DVT and initial human studies, a plane strain state appears to be a reasonable approximation for free-hand DVT scanning [3], [13].

Our basic approach has two steps. First, we derive the solution of the forward elastic problem in which the elastic properties of the object are known and the displacement and strain fields must be determined. Second, we use the solution of the forward problem to estimate the unknown Young's modulus spatial distribution in a small ROI based on an iterative comparison of theoretically predicted and ultrasonically measured longitudinal strain tensor components.

For a plane strain state, in-plane components u_r and u_φ of the displacement vector $\vec{U}$ are functions only of r and φ, and $u_z = 0$ [i.e., $\vec{U} = (u_r, u_\varphi, 0)$]. Hence, the two-dimensional (2-D) equations of static equilibrium must be satisfied [12]:

$$\begin{cases} \dfrac{\partial \sigma_{rr}}{\partial r} + \dfrac{1}{r}\dfrac{\partial \sigma_{r\varphi}}{\partial \varphi} + \dfrac{(\sigma_{rr} - \sigma_{\varphi\varphi})}{r} = 0 \\ \dfrac{\partial \sigma_{r\varphi}}{\partial r} + \dfrac{1}{r}\dfrac{\partial \sigma_{\varphi\varphi}}{\partial \varphi} + 2\dfrac{\sigma_{r\varphi}}{r} = 0 \end{cases}. \tag{1}$$

where σ_{st} is one component of the second ranked stress tensor. Assuming linear elasticity, the components of the stress tensor in an isotropic, continuous compressible medium are:

$$\begin{aligned} &\sigma_{st} = \lambda\theta\delta_{st} + 2\mu\varepsilon_{st} \quad s,t = r,\varphi, \\ &\lambda = \frac{E\nu}{(1-2\nu)(1+\nu)},\ \mu = \frac{E}{2(1+\nu)}, \\ &\theta = div\vec{U} = \varepsilon_{rr} + \varepsilon_{zz} + \varepsilon_{\varphi\varphi}, \end{aligned} \tag{2a}$$

$$\varepsilon_{rr} = \frac{\partial u_r}{\partial r},\ \varepsilon_{\varphi\varphi} = \frac{1}{r}\frac{\partial u_\varphi}{\partial \varphi} + \frac{u_r}{r},$$
$$\varepsilon_{r\varphi} = \frac{1}{2}\left(\frac{1}{r}\frac{\partial u_r}{\partial \varphi} + \frac{\partial u_\varphi}{\partial r} - \frac{u_\varphi}{r}\right), \tag{2b}$$
$$\varepsilon_{zz} = \varepsilon_{\varphi z} = 0,$$

where δ_{st} is the Kronecker delta symbol, λ and μ are the longitudinal and shear elastic modulus, respectively, ν is the Poisson's ratio, E is the Young's modulus, and ε_{st} is a component of strain tensor. The solution of the forward elastic problem (1), (2) for a compressible medium containing a homogeneous cylindrical inclusion under uniaxial load was originally presented in [14].

Most soft tissues and tissue-liked materials are very close to incompressible [15], i.e., the longitudinal elastic modulus λ is very large compared to the shear modulus and the divergence θ is very small. The product $\lambda\theta$ is finite and is recognized as the internal pressure in an incompressible, or nearly incompressible, material. This product must be eliminated from the equilibrium equations to stabilize elasticity reconstruction [11], [16]. Here we consider only incompressible media, i.e., Poisson's ratio equals 0.5, leading to the following simplification of (2):

$$\begin{aligned} &\theta = div\vec{U} = 0,\\ &\sigma_{st} = P\,\delta_{st} + 2\mu\varepsilon_{st}\\ &s,t = r,\varphi,\\ &P = \lim_{\substack{\lambda\to\infty\\ \theta\to 0}} \lambda\theta, \end{aligned} \tag{3}$$

where P is the static internal pressure. Also, for incompressible media $\mu = 3E$ and only one modulus (μ) describes the elastic properties of the material.

The generalization of Goudier's solution for uniaxially loaded incompressible media having an inhomogeneous cylindrical inclusion is presented in [8]. Here we present solutions to this problem for inhomogeneous objects under both uniaxial and shear-type loads.

First, consider uniaxial loading of the object for the case in which the direction $\varphi = 0$ is parallel to the direction of an applied deformation, as illustrated in Fig. 1. The solution of the forward problem (1)–(3) for a homogenous medium in this case has the form: $u_y = \varepsilon_0 y$, $u_x = -\varepsilon_0 x$, in Cartesian coordinates (x, y), in which the direction $\varphi = 0$ is parallel to the y direction, and $u_r = \varepsilon_0 r\cos(2\varphi)$, $u_\varphi = -\varepsilon_0 r\sin(2\varphi)$ in cylindrical coordinates (r, φ). Here ε_0 is the normal strain applied at infinity.

Noting these forms for the homogeneous case, the solution of (1)–(3) for a uniaxially loaded inhomogeneous medium has been found in [8]:

$$\begin{aligned} u_r &= u(r)\cos(2\varphi),\\ u_\varphi &= v(r)\sin(2\varphi),\\ P &= p_0(r) + p_1(r)\cos(2\varphi). \end{aligned} \tag{4}$$

Here $p_0(r)$ and $p_1(r)$ are unknown functions of r with $u(r)$ and $v(r)$ components.

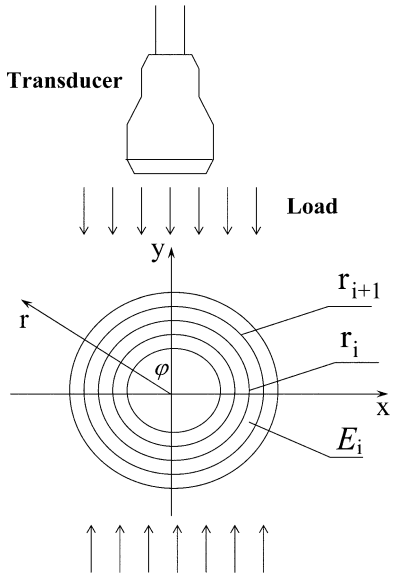

Fig. 1. Schematic representation of DVT deformation in which a blood clot containing vessel is modeled as a long cylinder. The direction of external loading is parallel to the axial direction of ultrasound beam. The centers of both cylindrical (r, φ) and Cartesian (x, y) systems of coordinates are placed in the center of the vessel, and the z-axis is aligned with the longitudinal axis of the vessel. The region of interest is divided in multiple rings with constant Young's modulus E_i within each ring.

Using the incompressibility condition, the displacement components are related as:

$$v = -\frac{1}{2}\left(u + r\frac{du}{dr}\right). \tag{5}$$

As noted in [8], assuming that $E = E(r)$, substituting (4) and (5) into (1)–(3) and eliminating the pressure, an equation coupling $u(r)$ and $E(r)$ is obtained:

$$r^4\frac{d^4u}{dr^4} + a_3r^3\frac{d^3u}{dr^3} + a_2r^2\frac{d^2u}{dr^2} + a_1r\frac{du}{dr} + a_0u = 0, \tag{6}$$

with

$$\begin{aligned} a_0 &= 3(r^2\Gamma + \gamma r + 3),\\ a_1 &= r^2\Gamma - 7\gamma r - 9,\\ a_2 &= r^2\Gamma + 7\gamma r - 3,\\ a_3 &= 2(3 + \gamma r), \end{aligned}$$

where

$$\gamma = \frac{1}{E}\frac{dE}{dr},\ \Gamma = \frac{1}{E}\frac{d^2E}{dr^2}.$$

At infinity, the inclusion cannot influence the deformation pattern. Consequently, the boundary condition for (6) at infinity should be the same as for loading a homogeneous medium. Hence:

$$u(0) = 0 \text{ and } \lim_{r\to\infty}\left[\frac{u(r)}{r}\right] \to \varepsilon_0, \tag{7}$$

where ε_0 is the uniform normal strain at infinity.

Because the deformation of soft tissues *in vivo* can be modeled, in general, by a combination of uniaxial and shear-type loads, the forward problem for shear-type loading of an inhomogeneous object must be solved in addition to the solution presented above. For shear-type loading of a homogeneous object, when the x-axis (see Fig. 1) is parallel to the direction of an applied deformation, the solution of the forward problem (1)–(3) has the form: $u_y = 0$, $u_x = 2\varepsilon_1 y$, in Cartesian coordinates (x, y) and $u_r = -\varepsilon_1 r \sin(2\varphi)$, $u_\varphi = -\varepsilon_1 r[1 + \cos(2\varphi)]$ in cylindrical coordinates (r, φ). Here ε_1 is the shear deformation applied at infinity.

Noting these solutions for the homogeneous case, we attempt to find the solution of (1)–(3) for an inhomogeneous medium of form:

$$\begin{aligned} u_r &= u(r)\sin(2\varphi), \\ u_\varphi &= \mathsf{v}_0(r) + \mathsf{v}_1(r)\cos(2\varphi), \\ P &= p_0(r) + p_1(r)\sin(2\varphi). \end{aligned} \tag{8}$$

The incompressibility condition in this case leads to:

$$\mathsf{v}_1 = \frac{1}{2}\left(u + r\frac{du}{dr}\right). \tag{9}$$

Substituting (8) and (9) into (1)–(3) two equations are obtained to determine the unknown functions u and v_0. For unknown u the equation has the same form (6) as the case of normal loading. For unknown v_0 the following equation must be solved:

$$\gamma\left(\frac{d\mathsf{v}_0}{dr} - \frac{\mathsf{v}_0}{r}\right) + \left(\frac{d^2\mathsf{v}_0}{dr^2} + \frac{1}{r}\frac{d\mathsf{v}_0}{dr} - \frac{\mathsf{v}_0}{r^2}\right) = 0. \tag{10}$$

The general solution of this equation is:

$$\mathsf{v}_0 = A\left[(\gamma - 1/r)e^{-\gamma r} + r\gamma^2 \int \frac{e^{-\gamma r}}{r} dr\right] + Cr,$$

where A and C are arbitrary constants.

Noting that the value $\mathsf{v}_0(0)$ must be finite, the solution of (10) takes the form $\mathsf{v}_0 = Cr$. Like the normal loading case, the boundary condition for (6) at infinity should be the same as shear loading of a homogeneous medium:

$$u(0) = 0 \text{ and } \lim_{r\to\infty}\left[\frac{u(r)}{r}\right] \to -\varepsilon_1, \tag{11}$$

where ε_1 is the uniform shear strain at infinity. Therefore, in both cases (uniaxially or shear-type loaded object) if the distribution $E(r)$ is known, the forward problem is reduced to solving a single ordinary differential equation, i.e., (6). That is, (6) is the general equation coupling the elasticity distribution with the magnitude of the radial displacement independent of the deformation type.

To solve (6), various numerical procedures can be used (for example, Runge-Kutta method). However, if the Young's modulus is constant within some interval $[r_1, r_2]$, the analytic solution of (6) can be derived. In this case, the coefficients a_i are constant and (6) has the form:

$$r^4\frac{d^4u}{dr^4} + 6r^3\frac{d^3u}{dr^3} - 3r^2\frac{d^2u}{dr^2} - 9r\frac{du}{dr} + 9u = 0. \tag{12}$$

The solution in this interval reduces to:

$$u(r) = Ar + Br^3 + \frac{C}{r} + \frac{D}{r^3}, \tag{13}$$

where A, B, C, and D are arbitrary constants. This fact can be used to greatly simplify the procedure to reconstruct $E(r)$.

To find the general solution of (6) for arbitrary $E(r)$ over a ROI, we assume that the Young's modulus is constant within each subinterval $[r_i, r_{i+1}]$, i.e., we assume that $E(r) = E_i = const$, $r \in [r_i, r_{i+1}]$, $i = 1 \ldots N$, where N is the total number of subintervals covering the region of interest (see Fig. 1). Therefore, (13) becomes:

$$u(r) = A_i r + B_i r^3 + \frac{C_i}{r} + \frac{D_i}{r^3},\ i = 1 \ldots N. \tag{14}$$

In general, the values E_i and unknown constants A_i, B_i, C_i, and D_i are different for each ring $[r_i, r_{i+1}]$. These unknown constants can be found using boundary conditions (7) or (11) and the stress and displacement continuity conditions at the ring boundaries:

$$\begin{aligned} [\sigma_{rr}]_{r=r_i} = 0,\ [\sigma_{r\varphi}]_{r=r_i} = 0, \\ [u_r]_{r=r_i} = 0,\ [u_\varphi]_{r=r_i} = 0, \end{aligned} \tag{15}$$

where the notation $[f]_{r=r_i}$ means $f_{r=r_i+\Delta} - f_{r=r_i-\Delta}$ for vanishing Δ. Note that any continuous function $E(r)$ can be accurately approximated in this way. The solution of (6) is greatly simplified because only the linear system of algebraic equations for unknowns A_i, B_i, C_i, and D_i, $i = 1 \ldots N$ needs to be solved to find the solution of the forward elastic problem.

It is well-known that signal-to-noise ratio (SNR) of axial displacement measurements is higher than that of lateral displacements [17]–[19]. Here we will use only one experimentally measured axial (in Cartesian coordinates) component of the strain tensor $\varepsilon_{yy} = \frac{\partial u_y}{\partial y}$ to solve the inverse problem.

The form of the analytic solutions to the forward elastic problems can be used to further simplify DVT elasticity reconstruction based on measured images of ε_{yy} (i.e., $\varepsilon_{yy}^{\exp}$). First, using the approach presented above, one can conclude that the distribution ε_{yy} corresponding to uniaxial loading along the line having the angle $\alpha + \pi/4$ and the distribution corresponding to shear deformation perpendicular to the line having the angle α are the same if $\varepsilon_0 = -\varepsilon_1$. Therefore, shear-type loading need not be treated separately but can be replaced by a corresponding uniaxial loading.

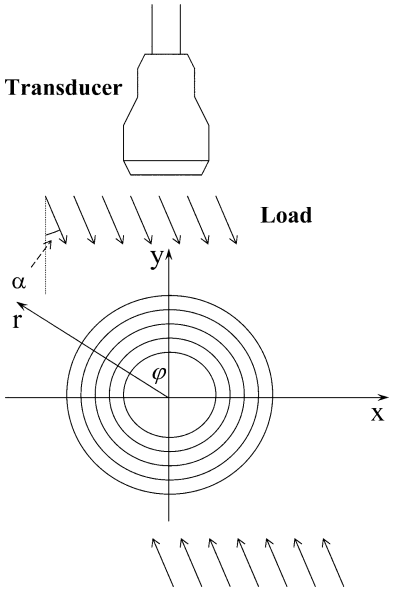

Fig. 2. Schematic representation of DVT deformation. In this model, the external load is applied at an angle α relative to the axial direction of an ultrasound beam. Indeed, during free-hand triplex ultrasound, the direction of the surface applied deformation may not coincide with the axial direction of the ultrasound beam.

Second, the set of uniaxial loadings $\varepsilon_0^k, k = 1 \dots K$ along the different axes α_0^k can be replaced by one effective uniaxial loading ε_0 along a certain axis α where:

$$|\varepsilon_0| = \left\{ \left[\sum_{k=1}^{K} \varepsilon_0^k \cos(2\alpha_k) \right]^2 + \left[\sum_{k=1}^{K} \varepsilon_0^k \sin(2\alpha_k) \right]^2 \right\}^{1/2},$$

$$\tan(2\alpha) = \sum_{k=1}^{K} \varepsilon_0^k \sin(2\alpha_k) \Big/ \sum_{k=1}^{K} \varepsilon_0^k \cos(2\alpha_k).$$

More complex deformations, when several uniaxial and shear loadings are applied, can be reduced to one uniaxial loading at a certain angle. Therefore, to model longitudinal strain fields within the object, only one uniaxial effective deformation ε_0 applied along the angle α is needed (Fig. 2).

B. Inverse Problem

Having experimentally measured the axial strain component $\varepsilon_{yy}^{\exp}$ and using the analytic solution of the forward problem for a given deformation, elasticity reconstruction can be posed as a minimization problem. Given the Young's moduli over a set of rings, the center of the vessel (x_0, y_0) (i.e., the origin of the coordinate system), the angle α and the effective deformation at infinity ε_0 applied along this angle, we can compute the theoretical distribution of axial strain. The unknown Young's modulus E_i can be estimated by minimizing the difference between theoretically predicted and experimentally measured strain images [13]. In general, α, ε_0, and the center (x_0, y_0) of the vein also are unknown and must be estimated simultaneously with the unknown E_i by minimizing the error function. Therefore, the error function takes the form:

$$\delta = \left\| \varepsilon_{yy}^{\exp} - \varepsilon_{yy}^{\text{theory}}(E_i, \varepsilon_0, \alpha, x_0, y_0) \right\|, \qquad (16)$$

and elasticity reconstruction reduces to a simultaneous minimization of the error function of (16) with respect to the unknown elasticity distribution, the position of the origin of the coordinate system, the direction of the effective uniaxial loading of the object, and the magnitude of the net effective deformation along this direction.

Although the loading angle α must be estimated as part of the reconstruction procedure, its value does not greatly affect the reconstructed elasticity distribution over a wide angular range. This can be explained as follows. The analytic solution for the longitudinal strain component for uniaxial loading in Cartesian coordinates is:

$$\varepsilon_{yy}^{\text{theory}} = \varepsilon_0 [R \sin(2\alpha) + Q \cos(2\alpha)],$$

where

$$R = \frac{\overline{x}\,\overline{y}}{2r^5}\left(r^2 - 2\overline{y}^2\right)\left(3u - 3r\frac{du}{dr} + r^2\frac{d^2u}{dr^2}\right),$$

$$Q = -\frac{1}{r^5}\left[3u\overline{x}^2\overline{y}^2 + r\frac{du}{dr}\left(\overline{x}^4 - \overline{x}^2\overline{y}^2 + \overline{y}^4\right) + r^2\frac{d^2u}{dr^2}\overline{x}^2\overline{y}^2\right],$$

$$\overline{x} = x - x_0,\ \overline{y} = y - y_0,$$

and $u(r)$ is the solution of (6) corresponding to the boundary condition $\lim_{r\to\infty}\left[\frac{u(r)}{r}\right] \to 1$ (i.e., unit strain at infinity). As part of the error minimization procedure, the partials of the error function with respect to α and ε_0 must satisfy $\partial\delta/\partial\varepsilon_0 = 0$ and $\partial\delta/\partial\alpha = 0$, which leads to:

$$\alpha = \frac{1}{2}\arctan\frac{\psi_2\varphi_2 - \psi_3\varphi_1}{\psi_2\varphi_1 - \psi_1\varphi_2},$$

$$\varepsilon_0 = \frac{\sin(2\alpha)\varphi_1 + \cos(2\alpha)\varphi_2}{\sin^2(2\alpha)\psi_1 + 2\sin(2\alpha)\cos(2\alpha)\psi_2 + \cos^2(2\alpha)\psi_3},$$

where

$$\psi_1 = \int_S R^2 ds,\ \psi_2 = \int_S RQ ds,\ \psi_3 = \int_S Q^2 ds,$$

$$\varphi_1 = \int_S \varepsilon_{yy}^{\exp} R ds,\ \varphi_2 = \int_S \varepsilon_{yy}^{\exp} Q ds,$$

and S is the area of the ROI.

By substituting these results for unknowns α and ε_0 into (16), the error function depends only on the origin of Cartesian coordinates and $u(r)$. Therefore, the unknown elasticity distribution $E(r)$ is coupled with $u(r)$ by the basic differential equation in (6) independent of the angle α, and the quality of elasticity reconstruction (i.e., contrast in terms of elasticity) depends only on the SNR in $\varepsilon_{yy}^{\exp}$ images.

To further understand the effect of the uniaxial deformation angle α on normal strain images, the analytic solution for the case of a homogenous cylindrical inclusion of Young's modulus E_1 bounded within an otherwise homogenous medium with Young's modulus $E_0 = E_1/2$ is presented in Figs. 3 and 4. Fig. 3 show images of the vertical normal strain ε_{yy} at several different values of the

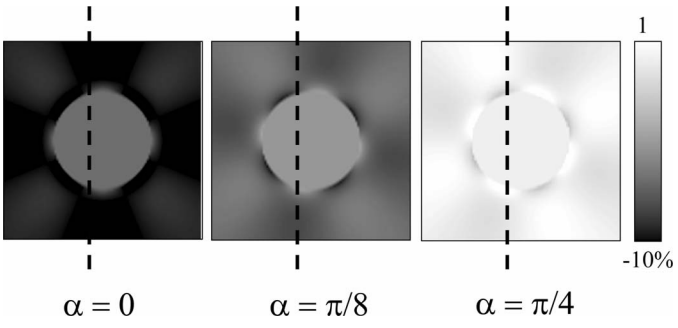

Fig. 3. Images of the normal, axial strain component (ε_{yy}) of a homogeneous cylindrical inclusion that is two times harder than an otherwise homogeneous background. In the analytical solution used to create these images, the external load was applied at (left) $\alpha = 0$, (center) $\alpha = \pi/8$, and (right) $\alpha = \pi/4$ relative to the axial direction of an ultrasound beam. The strain profiles along the dotted lines are presented in Fig. 4.

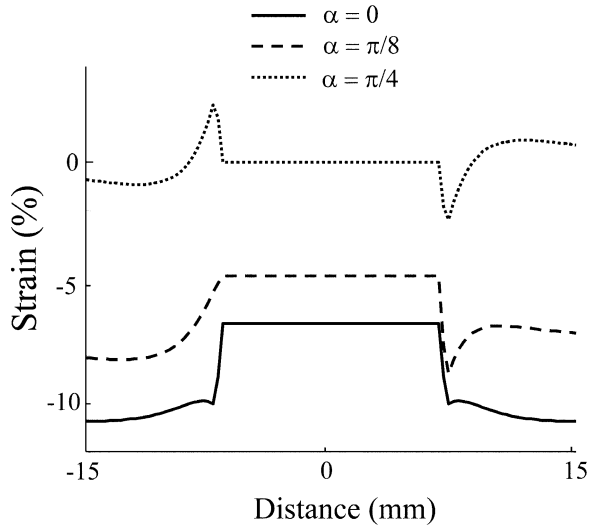

Fig. 4. Strain profiles through the vertical lines denoted in strain images in Fig. 3 are contrasted for quantitative comparison.

deformation angle α. Note that almost all contrast is lost as α approaches $\pi/4$. Profiles of single lines through these same images are presented in Fig. 4. Again, note the almost complete loss of contrast at $\alpha = \pi/4$. That is, if the net in-plane deformation can be approximated as a uniaxial load at angle $\alpha = \pi/4$, the inclusion is barely detectable by strain images alone. Model-based elasticity reconstruction is independent of α, consequently, full contrast can be recovered. Of course, reconstruction of the elasticity distribution is limited by the SNR in $\varepsilon_{yy}^{\exp}$ images. Nevertheless, elasticity reconstruction can recover contrast even as α differs significantly from 0. This is especially important for free-hand external loading, which most probably will be used in clinical experiments.

Unknown scalar parameters were estimated numerically using (16) by an iterative minimization procedure similar to the one used in [16]. One unknown was varied at a time, and iterative parameters which determine step size were chosen taking into account the second order polynomial approximation of δ as a function of each individual E_i under the restriction of decreasing error. If successful on a step, the global linear prediction for all unknowns simultaneously was used after each iteration to reduce oscillation. As discussed in [16], this iterative minimization procedure is accurate and fast. The time needed to solve each particular problem is less than one minute on a low-end computer for a reasonable number of layers (≤ 50).

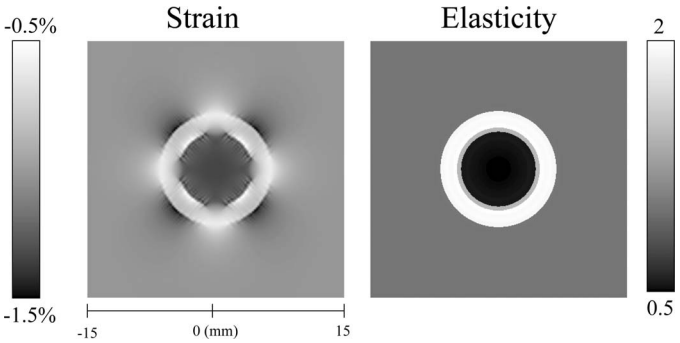

Fig. 5. Strain image and corresponding reconstructed elasticity image of DVT. The strain distribution was obtained using finite-element simulation (left) of the modeled DVT where the relative Young's modulus ratio for surrounding tissue, vessel wall, and clot is 1:2:0.5, respectively. The resulted strain distribution was then used as input into the reconstruction to obtain the elasticity image (right) that is closely depicting the original Young's modulus distribution.

III. Simulation

As an initial test of the reconstruction procedure outlined above, finite element 2-D simulations were performed on a simple model of DVT elasticity. This model assumed a finite thickness blood vessel of elastic modulus E_1 surrounded by a homogeneous medium with elastic modulus E_0. The lumen of the vessel contained a homogeneous clot, and the elastic modulus E_2 was varied to simulate both acute and chronic cases. All studies presented here used a commercial software package (Abaqus, HKS Inc., Pawtucket, RI) to solve the forward problem given the elasticity distribution and the boundary conditions. The computed noise-free axial strain tensor component $\varepsilon_{yy}(x, y)$ across the uniaxially loaded object were used as input for elasticity reconstruction. An acute clot was modeled with surrounding tissue, vessel wall, and clot having relative Young's moduli of 1:2:0.5, respectively. On the top and bottom of the 30-mm by 30-mm phantom, a constant uniaxial deformation was assumed, and the sides of the object were assumed to be free. To solve the forward problem, a 200 by 200 element grid was used. Results of the numerical simulation acted as $\varepsilon_{yy}^{\exp}(x, y)$ in (16) to estimate the elasticity distribution. Forty-one rings were used to reconstruct the elasticity. Note that the boundaries r_i of these rings *do not need to match* the prescribed boundaries of the wall and clot.

Fig. 5 shows the strain image output by the finite element simulation (left) with the reconstructed elasticity distribution (right). In Fig. 6 a profile through the center of

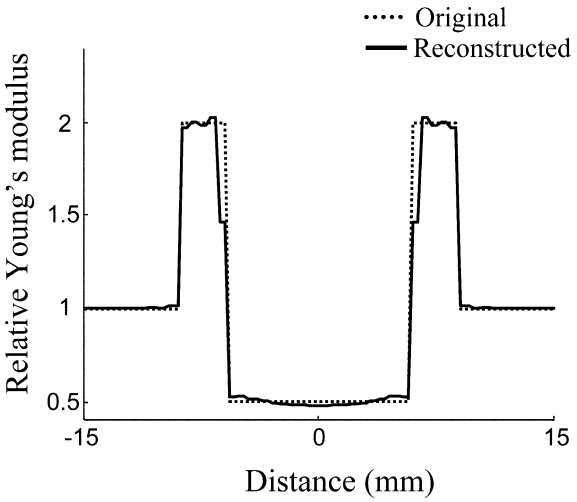

Fig. 6. Young's modulus distribution along a central vertical line of the reconstructed elasticity image presented in Fig. 5 contrasted with the original Young's modulus distribution used to generate input data for an elasticity reconstruction. Overall, reconstructed elasticity is in quantitative agreement with the original Young's modulus distribution.

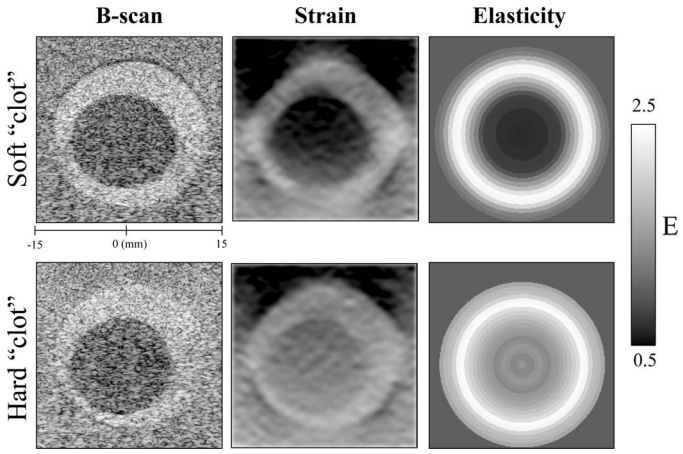

Fig. 7. Result of reconstructive elasticity imaging of acute (top) and chronic (bottom) DVT mimicking phantoms. The 40-mm by 40-mm B-scans (left column) are centered on the vessel and demonstrate the geometry of the hyperechoic vessel wall and hypoechoic blood clot. A 25% average surface deformation was applied to produce internal strains in the phantoms (center column). The strain distribution was used to reconstruct the Young's modulus distribution for both phantoms (right column) with a maximum number of layers not exceeding 21 for each phantom. Note that in both phantoms the clots are asymmetrically positioned within the veins; the model-based reconstruction assumes and, therefore, produces circularly symmetric elasticity maps.

the reconstructed image is compared to the actual modulus distribution used to produce the simulated strain image. Clearly, the reconstructed distribution closely matches the Young's modulus distribution used in the forward problem. Nearly identical results were obtained as the angle α was swept over $\pm 45°$. Of course, reconstructions near $\alpha = \pm 45°$ are meaningless for real data with finite SNR. Nevertheless, these results clearly indicate that the proposed reconstruction method is not highly sensitive to the form of in-plane loading. In addition, the influence of the boundary conditions on reconstruction is minimal, suggesting that model-based approach performs well for objects of finite size.

IV. Phantom Measurements

As a further test of the proposed reconstruction procedure, experiments were performed on a set of two tissue-equivalent gelatin phantoms modeling the DVT geometry. Each phantom was constructed in three steps. First a 125-mm by 100-mm by 75-mm rectangular homogeneous phantom was constructed using 6% by weight gelatin (300 Bloom type-A, Sigma Co., St. Louis, MO) and 0.5% by weight microspheres acting as ultrasonic scatterers (Amberlite Strongly Acidic Cation Exchanger, Sigma Co.). Second, a cylindrical hole 30 mm in diameter and 125 mm in length was made in the center of the phantom. It was filled with 12% by weight gelatin and 1% by weight microspheres to simulate a vessel wall. Third, a 19-mm diameter hole extending the length of the phantom was made in the center and filled with either 4% or 8% by weight gelatin and 0.5% by weight graphite flakes (Extra Fine Graphite, American Grease Stick Co., Muskegon, MI) to simulate soft (acute) and hard (chronic) clots. Both phantoms were constructed at the same time, and experiments were performed shortly after the phantoms were manufactured to avoid any undesired and uncontrolled changes in elasticity due to gel aging.

To deform the phantoms, the ultrasound array transducer was placed vertically into a custom holder attached to a unidirectional positioning slider (Velmex Inc., Bloomfield, NY) controlling vertical motion. Each phantom was centered in a tank so that the image plane of the transducer approximated the central plane, perpendicular to the longitudinal axis of the phantom. The tank was filled with water to provide contact between the array and phantom.

A Siemens Sonoline "Elegra" scanner (Siemens Medical Systems, Inc., Issaquah, WA) with a linear transducer array operating at 5 MHz (5.0HDPL40) was used to image and collect frames in real-time during continuous surface deformation. The average deformation of both phantoms was about 25%, and 83 frames were collected during the deformation. Strain images were obtained from these data using an adaptive, two-dimensional, phase-sensitive correlation speckle tracking algorithm [20], [21]. The correlation was computed using complex baseband signals with a kernel size of 1.28 mm (lateral) by 0.5 mm (axial). Complex correlation coefficients were filtered using a 1.28 mm (lateral) by 1 mm (axial) separable Hanning filter.

The ROI for reconstruction was chosen using B-scans. The B-scan and corresponding strain images of the phantom with soft and hard clots are presented in Fig. 7 (left and center columns, respectively). The size of the ROI was chosen as 40 mm by 40 mm. The Young's modulus was reconstructed by minimizing the error function (16) across

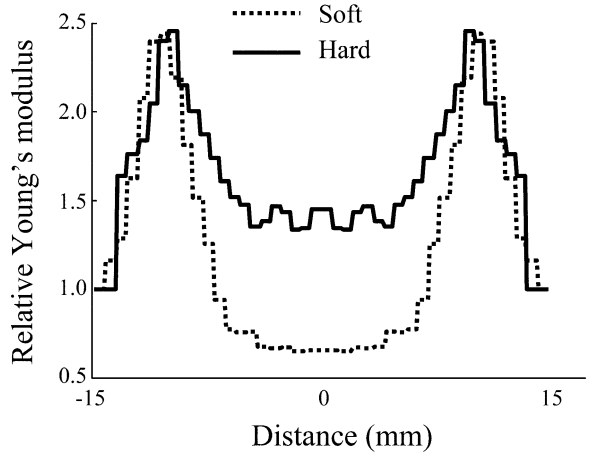

Fig. 8. Quantitative comparison of Young's modulus profiles through central line of elasticity images in Fig. 7. The surrounding tissue, vessel wall, soft and hard clot were produced using 6%, 12%, 4%, and 8% gelatin concentrations, respectively. The relative Young's modulus for these concentrations were 1.0:(2.65 ± 0.25):(0.5 ± 0.05):(1.53 ± 0.1), respectively, as determined independently by direct mechanical measurements. Clearly, reconstructed elasticity quantitatively agreed with independently measured elasticity of phantom materials.

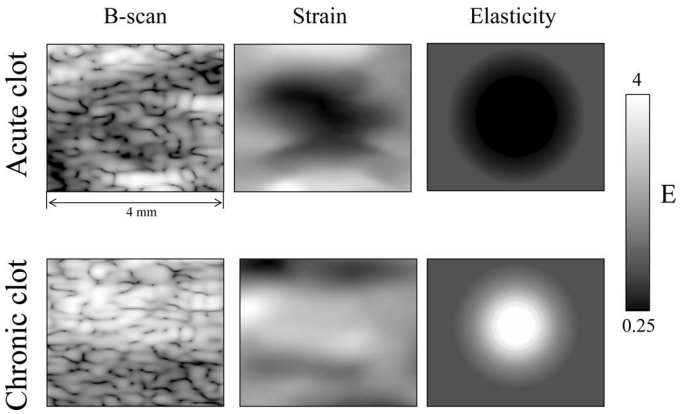

Fig. 9. Results of reconstructive elasticity imaging in Sprague-Dawley rats with stasis-induced acute (top) and chronic (bottom) DVT. The B-scans (left column) and images of axial strain (middle column) are displayed over the 4.5-mm by 3.7-mm ROI including a clot containing IVC, aorta, and a small portion of surrounding tissue. The strain images, displayed from −55% to −10%, suggest a significant difference between soft, 2-day-old clot (top) and hard, 9-day-old DVT (bottom). Elasticity images further confirm this observation but allow quantitative analysis of blood clot and vessel wall.

the ROI. Elasticity reconstruction starts with a homogeneous cylindrical inclusion (one layer), then the number of layers increases. The process is terminated when the relative difference between the last two steps becomes less then 2%. The maximum number of layers was 21 for each phantom.

The central profiles through the reconstructed elasticity images for the two phantoms are presented in Fig. 8. Approximately the same ratio of the elastic modulus of surrounding tissue to that of the wall is reconstructed in both cases, but the reconstructed Young's moduli of the clots differ.

To verify the results of elasticity reconstruction, the Young's modulus of the different phantom components was measured using a force-deformation system described in detail in [22]. Samples 75 mm by 25 mm by 50 mm in size were compressed by 15–20% such that a known surface displacement was produced. The resulting force was measured with a precision electronic balance. Boundary conditions for the samples were controlled to maintain a plane strain state. The relative Young's modulus for gelatin concentrations of 4%:6%:8%:12% were estimated as (0.5 ± 0.05):1.0:(1.53 ± 0.1):(2.65 ± 0.25). Again, the results of reconstruction are in good agreement with the results of independent direct measurements of the elastic properties of the phantom materials.

V. Animal Experiments

Animal studies were performed using a rat model of stasis induced venous thrombosis [23], [24]. Sprague-Dawley (*Rattus norvegicus*) rats (Harlan Sprague-Dawley, Inc., Indianapolis, IN) were anesthetized with isofluorane gas mixed with oxygen by a nose cone. Once anesthetized, a midline laparotomy was made, the small bowel was moved slightly to the left of the animal, and the inferior vena cava (IVC) was approached directly by careful blunt dissection. The IVC was ligated just below the level of the renal veins, with side and back branches also carefully isolated and ligated to ensure blood stasis and consistent thrombus formation, which occurs in over 90% of cases done by this method [23].

The animals then were kept for either 2 days or 9 days, corresponding to acute and chronic intervals, before undergoing ultrasound elasticity imaging studies. All animals developed clots as confirmed at the conclusion of the imaging studies, when rats were sacrificed and thrombosis was qualitatively characterized.

Prior to the imaging procedure, animals were anesthetized with isofluorane. A Siemens "Elegra" scanner with a linear, 7.5 MHz array ultrasound transducer (7.5L40) was used to image and collect several hundred consecutive frames of digital phase-sensitive ultrasound signals in real-time during continuous deformation of the rat's abdominal wall and underlying tissue. Details of this experiment are described in [4], [5]. Fig. 9 presents B-scans of acute (2-day) and chronic (9-day) clots (left column), the images of normal axial strain (center column) displayed from −55% to −10%, in which full black corresponds to −55% strain and lower, and full white corresponds to −10% strain and higher, and the results of elasticity reconstruction (right column). All images in Fig. 9 are 4.5 mm by 3.7 mm. The frame-to-frame displacements were computed using complex baseband signals with a correlation kernel size of 1.0 mm (lateral) by 0.2 mm (axial). The kernel size was chosen based on the full width at half maximum of its autocorrelation. To reduce peak hopping errors due to small kernel size, the adjacent cor-

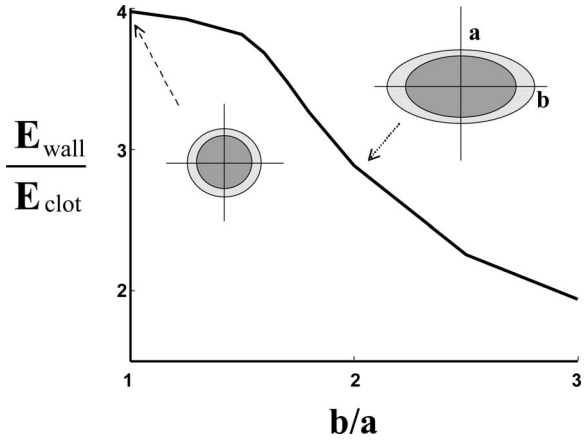

Fig. 10. Changes in elasticity contrast between vessel wall and blood clot due to the invalidity of the circular cross-section assumption used in the developed elasticity reconstruction model. In these finite-element simulations of the elliptically shaped vessel, the relative wall-to-clot Young's modulus $E_{\text{wall}}/E_{\text{clot}}$ was set to 4, and the eccentricity of the vessel with occluding blood clot was varied. The resulting strain images then were used in the elasticity reconstruction assuming a circular geometry of DVT. The resulted elasticity contrast is presented as a function of ellipse eccentricity suggesting that, for small deviations in geometry, the developed elasticity reconstruction technique is sufficient for quantitative aging of the blood clot.

relation functions were filtered using a 1.5 mm (lateral) by 1.0 mm (axial) separable Hanning filter. Axial strains were computed from accumulated axial displacements using a simple 1-D difference filter along the axial direction for correlation windows separated by 0.4 mm. The angle α was estimated as 11.7° for the acute case and −20° for the chronic case, small values consistent with the controlled nature of the deformation used for these studies. Acute and chronic clots clearly have very different elastic moduli. The chronic clot is harder by over an order of magnitude than the acute clot. Although further studies are needed to corroborate this initial result, the reconstructed images in Fig. 9 suggest that relative elasticity reconstruction may be able to age DVT.

VI. Discussion

All the results presented here assumed that the clot cross section was circular. This clearly was not the case for both phantom and animal studies. This also will not be the case for clinical scans. To test the valid range of the circular cross-section assumption, we used finite element simulations to create a set of strain fields for an elliptical model of DVT. These strain images were input to the reconstruction program assuming a circular DVT geometry. Results of the clot's Young's modulus reconstruction are presented in Fig. 10 as a function of ellipse eccentricity. For this simulation, the relative Young's modulus $E_{\text{wall}}/E_{\text{clot}}$ was assumed to be 4. For eccentricities reaching approximately 1.7, the error in the reconstructed elasticity is small. Above this value, the error smoothly increases at a fairly slow rate. An eccentricity of 1.7 is much larger than that seen in the animal studies presented here, and it is larger than expected in clinical studies based on the limited set of human scans done to date [13]. Consequently, the circular cross-section assumption is not expected to produce significant errors in reconstruction of the relative Young's modulus in human DVT.

It is also interesting to note that, in the human case, the posterior surface against which the pushing or deformation is performed is the femoral shaft. This distal surface is not flat and parallel to the ultrasound scanhead face, as is assumed in this model, but it is actually curved itself. Pushing against this curved surface will inevitably introduce components of shear in any deformation. The resistance of the described method to such effects should further add to the robustness of this technique *in vivo*.

This study also assumed that the clot's elastic properties are circularly symmetric (i.e., independent of angle). This is clearly not the case for a complex, heterogeneous clot. The symmetry assumption tends to average the elastic modulus, imposing an artificial low-pass filtering on the reconstructed image. This should not be a large practical concern because the primary motivation of the proposed reconstruction procedure is to properly represent the average elastic contrast between clot, vein wall, and surrounding tissue independent of loading details.

The model-based reconstruction technique presented here uses an analytic solution. This solution was derived under the assumptions of small strains in linear elastic materials. These assumptions, however, are not valid for large deformations. We demonstrated previously [16] that linear and nonlinear strain models of elasticity reconstruction are possible, where both approaches produced comparable results up to internal strain magnitudes of about 20%. Internal strains in our numerical and phantom experiments were in this range. The strains in animal studies were larger, indicating underestimated elasticity contrast if linear strains were used in elasticity reconstruction.

Another important problem for DVT aging is estimating the absolute value of the Young's modulus. With the present approach we can obtain only the relative Young's modulus reconstruction. For ultimate application as a general diagnostic technique, absolute elasticity may be needed. One approach is to include into the reconstruction procedure the information about the distribution of surface stress or pressure in response to surface applied deformations. Future work will focus on this possibility to create a robust method of triplex scanning to detect, diagnose, and stage human DVT.

VII. Conclusion

The proposed model-based approach to DVT elasticity reconstruction has some clear advantages: only one component of the strain tensor is used; the minimization procedure is very fast and stable given the small number of unknown scalar parameters derived from an analytic solution of the forward elastic problem; and it is not highly

sensitive to the details of external loading, a characteristic especially important for free-hand external loading. The approach was demonstrated using numerical simulations and measurements on both tissue-equivalent phantoms and an animal model of DVT. These results suggest that elasticity reconstruction may prove to be a practical adjunct to triplex scanning to detect, diagnose, and stage human DVT.

Acknowledgments

The authors would like to thank Siemens, Inc., for equipment access and technical support. The authors also would like to thank Ramon Erkamp for his contribution to direct elasticity measurements, and Dr. Myers, Brian Knipp, Shirley Wrobleski, and Dr. Wakefield for their help with animals studies.

References

[1] S. Y. Emelianov, J. M. Rubin, X. Chen, A. R. Skovoroda, T. W. Wakefield, and M. O'Donnell, "Ultrasound elasticity imaging of deep venous thrombosis," in *Proc. IEEE Ultrason. Symp.*, 2000, pp. 1791–1794.

[2] J. M. Rubin, S. R. Aglyamov, A. R. Skovoroda, D. Myers, S. Wrobleski, T. W. Wakefield, M. O'Donnell, and S. Y. Emelianov, "Ultrasound elasticity imaging of venous thrombosis," in *First International Conference on the Ultrasonic Measurement and Imaging of Tissue Elasticity*, 2002, p. 56.

[3] S. Y. Emelianov, X. Chen, M. O'Donnell, B. Knipp, D. Myers, T. W. Wakefield, and J. M. Rubin, "Triplex ultrasound: Elasticity imaging to age deep venous thrombosis," *Ultrasound Med. Biol.*, vol. 28, pp. 757–767, 2002.

[4] J. Hirsh and J. Hoak, "Management of deep vein thrombosis and pulmonary embolism. A statement for healthcare professionals. Council on Thrombosis (in consultation with the Council on Cardiovascular Radiology)," *Circulation*, vol. 93, no. 12, pp. 2212–2245, 1996.

[5] B. D. Lewis, "The peripheral veins," in *Diagnostic Ultrasound*. 2nd ed. C. M. Rumack, S. R. Wilson, and J. W. Charboneau, Eds. St. Louis, MO: Mosby, 1998, pp. 946–954.

[6] T. M. Hyers, G. Agnelli, R. D. Hull, J. G. Weg, T. A. Morris, M. Samama, and V. Tapson, "Antithrombic therapy for venous thromboembolic disease," *Chest*, vol. 114, Suppl. 5, pp. 561S–578S, 1998.

[7] R. D. Hull, G. E. Raskob, D. Rosenbloom, A. A. Panju, P. Brill-Edwards, J. S. Ginsberg, J. Hirsh, G. J. Martin, and D. Green, "Heparin for 5 days as compared with 10 days in the initial treatment of proximal venous thrombosis," *New Eng. J. Med.*, vol. 322, pp. 1250–1264, 1990.

[8] A. R. Skovoroda, S. Y. Emelianov, M. A. Lubinski, A. P. Sarvazyan, and M. O'Donnell, "Theoretical analysis and verification of ultrasound displacement and strain imaging," *IEEE Trans. Ultrason., Ferroelect., Freq. Contr.*, vol. 41, pp. 302–313, 1994.

[9] F. Kallel and M. Bertrand, "Tissue elasticity reconstruction using linear perturbation method," *IEEE Trans. Ultrason., Ferroelect., Freq. Contr.*, vol. 15, no. 3, pp. 299–313, 1996.

[10] K. J. Parker, L. Gao, R. M. Lerner, and S. F. Levinson, "Techniques for elastic imaging: A review," *IEEE Engin. Med. Biol. Magazine*, vol. 15, no. 6, pp. 52–59, 1996.

[11] A. R. Skovoroda, S. Y. Emelianov, and M. O'Donnell, "Tissue elasticity reconstruction based on ultrasonic displacement and strain images," *IEEE Trans. Ultrason., Ferroelect., Freq. Contr.*, vol. 42, no. 4, pp. 747–765, 1995.

[12] S. Timoshenko and J. Goodier, *Theory of Elasticity*. New York: McGraw-Hill, 1951.

[13] S. R. Aglyamov, A. R. Skovoroda, J. M. Rubin, M. O'Donnell, and S. Y. Emelianov, "Young's modulus reconstruction in DVT elasticity imaging," *Ultrason. Imag.*, vol. 22, p. 174, 2002.

[14] J. N. Goodier, "Concentration of stress around spherical and cylindrical inclusions and flaws," in *J. Appl. Mech.*, vol. 55, no. 39, pp. 39–44, 1933.

[15] A. P. Sarvazyan, "Low frequency acoustic characteristics of biological tissues," *Mech. Polymers*, vol. 4, pp. 691–695, 1975.

[16] A. R. Skovoroda, M. A. Lubinski, S. Y. Emelianov, and M. O'Donnell, "Reconstructive elasticity imaging for large deformation," *IEEE Trans. Ultrason., Ferroelect., Freq. Contr.*, vol. 46, no. 3, pp. 523–535, 1999.

[17] M. A. Lubinski, S. Y. Emelianov, K. R. Raghavan, A. E. Yagle, A. R. Skovoroda, and M. O'Donnell, "Lateral displacement estimation using tissue incompressibility," *IEEE Trans. Ultrason., Ferroelect., Freq. Contr.*, vol. 43, pp. 247–255, 1996.

[18] A. R. Skovoroda, M. A. Lubinski, S. Y. Emelianov, and M. O'Donnell, "Nonlinear estimation of the lateral displacement using tissue incompressibility," *IEEE Trans. Ultrason., Ferroelect., Freq. Contr.*, vol. 45, pp. 491–503, 1998.

[19] E. E. Konofagou and J. Ophir, "A new method for estimation and imaging of lateral strains and Poisson's ratios in tissues," *Ultrasound Med. Biol.*, vol. 24, no. 8, pp. 1183–1199, 1998.

[20] M. A. Lubinski, S. Y. Emelianov, and M. O'Donnell, "Speckle tracking methods for ultrasonic elasticity imaging using short-time correlation," *IEEE Trans. Ultrason., Ferroelect., Freq. Contr.*, vol. 46, pp. 82–96, 1999.

[21] M. A. Lubinski, S. Y. Emelianov, and M. O'Donnell, "Adaptive strain estimation using retrospective processing," *IEEE Trans. Ultrason., Ferroelect., Freq. Contr.*, vol. 46, pp. 97–107, 1999.

[22] R. Q. Erkamp, P. Wiggins, A. R. Skovoroda, S. Y. Emelianov, and M. O'Donnell, "Measuring the elastic modulus of small tissue samples," *Ultrason. Imag.*, vol. 20, pp. 17–28, 1998.

[23] D. D. Myers, S. K. Wrobleski, P. K. Henke, and T. W. Wakefield, "Coagulation biology," in *Surgical Research*. W. Souba and D. Wilmore, Eds. San Diego, CA: Academic, 2001, pp. 989–1000.

[24] T. W. Wakefield, R. M. Strieter, C. A. Wilke, A. M. Kadell, S. K. Wrobleski, M. D. Burdick, R. Schmidt, S. L. Kunkel, and L. J. Greenfield, "Venous thrombosis-associated inflammation and attenuation with neutralizing antibodies to cytokines and adhesion molecules," *Arterioscler. Thromb. Vasc. Biol.*, vol. 15, pp. 258–268, 1995.

Salavat R. Aglyamov received the B.S. and M.S. degrees in applied mathematics in 1991 and 1993, respectively, from Moscow State University, Moscow, Russia. He received the Ph.D. degree in biomechanics in 1999 from Institute of Theoretical and Experimental Biophysics, Pushchino, Moscow region, Russia. From 1993 to the present he has been working at the Institute of Mathematical Problems in Biology, Pushchino, Moscow region, Russia. From 2001 to 2002 he worked in the Biomedical Ultrasonics Lab at the University of Michigan, Ann Arbor, as postdoctoral fellow, where he was engaged in mathematical modeling of behavior of the soft biological tissue under externally applied loading. He is currently a research fellow in the Department of Biomedical Engineering at the University of Texas at Austin.

His research interests are in the areas tissue biomechanics, applied mathematics and elasticity imaging.

Andrei R. Skovoroda received the B.S. and M.S. degrees in mathematics and mechanics in 1973 and 1975, respectively, from the Novosibirsk State University, Novosibirsk, Russia (formerly USSR), and the Ph.D. degree in 1985 from the Moscow State University, Moscow, Russia (formerly USSR).

From 1975 to 1977 he was a lecturer in theoretical mechanics at the College of Textile Technology, Barnaul, USSR. From 1977 to 1980 he was a Ph.D. researcher at the subfaculty of Plasticity of the Moscow State University, where he worked on the dynamic behavior of plates under blast-type loading. In 1981 he held an appointment as a junior research associate at the Laboratory of Mathematical Modeling of the

Research Computing Center of the USSR Academy of Sciences (the present name, Institute of Mathematical Problems of Biology, Russian Academy of Sciences), Pushchino, Russia, where he developed efficient mathematical methods to solve the differential equations of the theory of elasticity. In 1986 he became a senior research associate and was Scientific Secretary at the same Institute from 1988 to 1993. He was Head of the Laboratory of Mathematical Problems in Biomechanics and worked on the biomechanics of soft tissue in the late 1990s. From 1991 through his untimely death in 2003, Dr. Skovoroda was also a Visiting Research Scientist in the Biomedical Ultrasonics Lab at the University of Michigan, Ann Arbor.

Dr. Skovoroda authored and co-authored more than 90 articles for archival publications and papers presented at All-Union and international meetings.

Jonathan M. Rubin was born in May, 1947. He received a B.A. in Chemistry from the University of Utah in 1969. He received his M.D. from the University of Chicago Pritzker School of Medicine in 1974, and his Ph.D. in Biophysics and Theoretical Biology from the University of Chicago in 1977. From 1979 to 1984, Dr. Rubin was the director of the Section of Body Computed Tomography and Ultrasound Imaging in the Department of Radiology at the University of Chicago. He has been at the University of Michigan since 1984 where he is now a Professor of Radiology and the Division Director of Ultrasound Imaging. His research interests include ultrasound contrast agents, ultrasound flow imaging, ultrasound artifacts, elasticity imaging, and optoacoustic imaging.

Matthew O'Donnell (M'79–SM'84–F'93) received B.S. and Ph.D. degrees in Physics from the University of Notre Dame, Notre Dame, Indiana, in 1972 and 1976, respectively. Following his graduate work, Dr. O'Donnell moved to Washington University in St. Louis, MO, as a postdoctoral fellow in the Physics Department working on applications of ultrasonics to medicine and nondestructive testing. He subsequently held a joint appointment as a senior research associate in the Physics Department and a Research Instructor of Medicine in the Department of Medicine at Washington University. In 1980 he moved to General Electric Corporate Research and Development Center in Schenectady, NY, where he continued to work on medical electronics, including magnetic resonance and ultrasound imaging systems. During the 1984–1985 academic year, he was a Visiting Fellow in the Department of Electrical Engineering at Yale University, New Haven, CT, investigating automated image analysis systems. In a bold move during 1990, Dr. O'Donnell became a professor of electrical engineering and computer science at the University of Michigan in Ann Arbor, MI. Since 1997, he has held a joint appointment as Professor of Biomedical Engineering at Michigan, and in 1998 he was named the Jerry W. and Carol L. Levin Professor of Engineering. Currently, he is the Chair of the Biomedical Engineering Department.

His most recent work has explored new imaging modalities in biomedicine, including elasticity imaging, in vivo microscopy, opto-acoustic arrays, opto-acoustic contrast agents, microwave-induced ultrasonic imaging, and catheter-based devices.

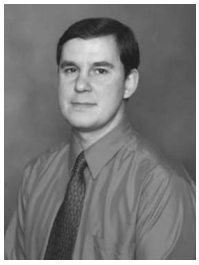

Stanislav Y. Emelianov (M'94) was born in May 1966. He received the B.S. and M.S. degrees in physics in 1986 and 1989, respectively, from the Moscow State University, Moscow, Russia (former USSR) and the Ph.D. degree in physics in 1993 from Moscow State University, and the Institute of Mathematical Problems of Biology Pushchino, Russia, of the Russian Academy of Sciences, Russia.

In 1989, he joined the Institute of Mathematical Problems of Biology, where he was engaged in both mathematical modeling of soft tissue biomechanics and experimental studies of noninvasive methods in medical diagnostics based on tissue elasticity variations. Following his graduate work, he moved to the University of Michigan, Ann Arbor, as a postdoctoral Fellow in the Bioengineering Program, and Electrical Engineering and Computer Science Department. From 1996 to 2002, Dr. Emelianov was a research scientist at the Biomedical Ultrasonics Laboratory at the University of Michigan. During his tenure at Michigan, he was involved primarily in the theoretical and practical aspects of elasticity imaging. Currently he is an assistant professor of Biomedical Engineering at the University of Texas at Austin.

His research interests are in the areas of medical imaging for therapeutics and diagnostic applications, cellular and molecular microscopy, elasticity imaging, opto-acoustical imaging, and radiation pressure imaging.